Strong spectral variation of biomass smoke light absorption and single scattering albedo observed with a novel dual wavelength photoacoustic instrument

Kristin Lewis[a,*], William P. Arnott[a], Hans Moosmüller[b], and Cyle E. Wold[c]

[a] *Department of Physics, University of Nevada, Reno, NV 89557, USA*
[b] *Desert Research Institute, Reno, NV 89512, USA*
[c] *Fire Sciences Laboratory, Missoula, MT 59808, USA*

[*] Corresponding author. Tel.: +1 775 784 4295; *E-mail address*: lewisk13@unr.nevada.edu

Abstract

A dual-wavelength photoacoustic instrument operating at 405 nm and 870 nm was used during the 2006 Fire Lab at Missoula Experiment (FLAME) to measure light scattering and absorption by smoke from the combustion of a variety of biomass fuels. Simultaneous measurements of aerosol light scattering by reciprocal nephelometry within the instrument's acoustic resonator accompany photoacoustic aerosol light absorption measurements. Single scattering albedo values at 405 nm ranging from 0.37 to 0.95 were measured for different fuel types, and the spectral dependence of absorption was quantified using the Ångström exponent of absorption. An absorption Ångström exponent near unity is commonly observed for motor vehicle emission-generated black carbon aerosol. For biomass smoke, Ångström exponents as high as 3.5 were found in association with smoke having single scattering albedo near unity. The measurements strongly suggest that light absorbing organic material is present in wood smoke. A second single wavelength photoacoustic instrument with reciprocal nephelometry was used to quantify aerosol scattering and absorption at 532 nm. Absorption Ångström exponents calculated using 532 nm and 870 nm data were as large as 2.5 for smoke with single scattering albedos near unity. The spectral variation in optical properties provides insight into differentiation of aerosol from mobile or industrial sources versus those from biomass burning. Optical properties of biomass smokes could be classified by general fuel type such as flowering shrubs versus pine needle litter.

1. Introduction

The optical properties of biomass burning aerosols are an important element in the complex system of atmospheric radiation transfer . Beyond the negative consequences that aerosols pose to human health and visibility, they also affect the lifetime of clouds, the hydrological cycle [*Ramanathan, et al.*, 2001], and the global radiation balance [*Horvath*, 1993; *Lohmann and Feichter*, 2005]. Biomass burning aerosols affect the radiation budget of the atmosphere by both absorbing and scattering light. They are composed of black carbon (BC), organic carbon (OC), and inorganic materials [*Reid, et al.*, 2005]. Sulfate and nitrate aerosols from anthropogenic sources, which predominately scatter radiation, are thought to be counteracting to some extent global warming caused by greenhouse gases such as carbon dioxide [*Charlson, et al.*, 1992]. Light absorbing particles, primarily produced by incomplete combustion of carbonaceous fuels and referred to as black carbon, have the opposite effect and warm the atmosphere. In fact, it has been proposed that the warming effect of carbonaceous aerosols may balance the cooling effect of scattering aerosols [*Jacobson*, 2001]. Uncertainties in the source magnitude, global distribution and mixing state of light absorbing aerosols compound the challenges of determining the role of aerosol in climate [*Andreae*, 2001].

Light absorbing carbon particles are the most abundant and efficient light absorbing components in the atmosphere in the visible spectrum. These particles are a product of incomplete combustion of carbon-based fuels such as from industrial processes, motor vehicles, and biomass burning. The complex morphology of carbonaceous soot particles is best described as fractal-like clusters of small spherules.

Soot optics can vary strongly with the number of monomers, monomer size, fractal dimension, and refractive index [*Chakrabarty, et al.*, 2006; 2007; *Liu, et al.*, 2007].

The term "brown carbon" refers to light absorbing organic carbon aerosol in the atmosphere [*Andreae and Gelencser*, 2006; *Sun, et al.*, 2007]. Absorption by organic species is strongly wavelength dependent, with increased absorption for ultra-violet and shorter-wavelength visible radiation, giving the particles a brownish hue. A clear distinction has been found, in terms of the band-gap relationship used to describe the carbon absorption spectrum, between black carbon and strongly absorbing organic carbon. The lowest band-gap energy, E_g, found for OC was E_g=1.6 eV; the E_g for BC is thought to be equal to zero [*Sun, et al.*, 2007]. *Sun et al*. [2007] describe the absorption spectrum using band gap and Urbach relationships instead of using the absorption Ångström exponent. We discuss primary OC and BC distinctions based on wavelength-dependent absorption, quantified by the absorption Ångström exponent.

Atmospheric aerosols have the potential to modify climate because they absorb and scatter radiation. There is much discussion as to the importance of light absorbing carbon as a driver for global warming [*Bond and Sun*, 2005]. Radiative forcing by light absorbing carbon aerosol has been found by some modeling studies to be comparable in magnitude to that of CH_4, rivaling the cooling effects of sulfate and nitrate aerosols [*Jacobson*, 2001], while a lesser climate effect is found by others [*Jones, et al.*, 2005]. Due to its light scattering properties, OC is generally thought to have a negative forcing effect on climate. However, some organic constituents in carbonaceous aerosols also absorb radiation, with strongest absorption at shorter solar radiation wavelengths where the impact on atmospheric photochemistry is significant.

Emissions from biomass burning are a large source of atmospheric BC aerosol and particulate organic matter. For example, from 1990 to 2000 the global contribution of open vegetation burning and biofuel combustion emissions to BC and organic aerosols was larger than that from the burning of fossil fuels [*Ito and Penner*, 2005]. Biomass burning in the tropics introduces large amounts of smoke particles into the atmosphere, providing cloud condensation nuclei that alter the microphysical and radiative properties of tropical clouds and rain systems [*Crutzen and Andreae*, 1990]. Smoke over the Amazon Basin was found to increase cloud reflectivity and reduce cloud droplet size [*Kaufman and Fraser*, 1997]. These changes, which serve to make clouds brighter and less efficient at releasing precipitation, lead to rain suppression, reduction in the amount of sunlight reaching the surface of the Earth, and result in solar heating of the atmosphere [*Ramanathan, et al.*, 2001].

The spectral dependence of biomass burning smoke absorption and scattering coefficients is needed for interpretation of optical remote sensing measurements and for modeling of aerosol forcing of climate and photochemistry. Measurements of light absorption by atmospheric particles are generally made at a single wavelength. Absorption at additional solar wavelengths is then extrapolated assuming a power-law relationship between aerosol absorption coefficient, β_{abs}, and radiation wavelength, λ:

$$\beta_{abs} = a\lambda^{-b}. \qquad \text{(Eq. 1)}$$

Here a is independent of wavelength and b is the Ångström exponent of absorption. Absorption of visible radiation by BC is generally thought to have an inverse relationship

to wavelength, or $\beta_{abs} \sim \lambda^{-1}$. An Ångström exponent of one implies a wavelength-independent refractive index for BC and particle size much smaller than the wavelength [*Bergstrom, et al.*, 2002]. Particles from diesel combustion have been shown to display a weak wavelength dependence on absorption, with *b* equal to approximately one [*Schnaiter, et al.*, 2003]. A stronger spectral dependence on absorption, characterized by Ångström exponent values greater than 1, has been found for other aerosol species. The increased Ångström exponent values result from stronger absorption at shorter wavelengths. Particles emitted from low-temperature combustion of coal [*Bond*, 2001] and lignite [*Bond, et al.*, 1999b] exhibit wavelength-dependent absorption with measured *b* values as high as 3.0. Smoldering combustion of pine needles also produces non-BC particulate matter with a strong spectral dependence on absorption [*Patterson and McMahon*, 1984]. The OC component of aerosols exhibits enhanced absorption at wavelengths shorter than 600 nm. Recently, *Kirchstetter et a*l. [2004] used a filter-based method to measure aerosol light absorption for particles from biomass and motor vehicle combustion. They found light absorption by aerosols from motor vehicles varied approximately as λ^{-1}, as expected for BC-dominated particles. However, an Ångström exponent of approximately $b = 2$ was found to be appropriate for smoke aerosols from burning African savannah grass. This stronger spectral dependence was strongly diminished when OC was extracted from the biomass smoke aerosol samples. Ångström exponents between 2.2 and 3.5 were also deduced for aerosols from propane combustion with high OC content [*Schnaiter, et al.*, 2006]. All of the afore cited Ångström exponents were calculated using absorption measurements at 450 nm and 550 nm with the exception of those reported by *Kirchstetter et a*l. [2004], which were determined over

different wavelength regions for each sample (e.g., 330 nm and 1000 nm for one savannah fire).

The single-scattering albedo, ω, is defined as the ratio of the scattering coefficient, β_{sca}, to the extinction coefficient, β_{ext}, where the extinction coefficient is the sum of absorption and scattering coefficients,

$$\omega \equiv \frac{\beta_{sca}}{\beta_{ext}} = \frac{\beta_{sca}}{\beta_{abs} + \beta_{sca}}. \qquad \text{(Eq. 2)}$$

This is a useful qualitative parameter for estimating radiative properties of an aerosol, particularly the net forcing (cooling or warming) effect an aerosol will have on the atmosphere. Single scattering albedo measurements for each of the different biomass smoke aerosols are reported at wavelengths of 405 nm and 532 nm. The single scattering albedo was found to range from 0.377 to 0.954 at 405 nm, with lower values associated with burning bushes and tree limbs. Larger values were associated with smoldering grass and pine needle fuels.

2. Fire Laboratory at Missoula Experiment (FLAME)

Laboratory measurements of biomass smoke optical properties were made at the United States Forest Service Fire Sciences Laboratory in Missoula, Montana in June 2006. The Fire Lab at Missoula Experiment (FLAME) has the primary goal of characterizing particulate matter emissions by wildland fires relevant to visibility impairment and PM non-attainment [*Moosmüller, et al.*, 2007]. Project findings support the needs of wildland fire managers and policy makers in determining the contribution of biomass burning to PM2.5 and visibility on a regional basis, focusing on the western and

southeastern U.S. regions. Project goals include a greater understanding of the optical properties of fire emissions, as well as optical property and particulate matter (PM) emission rates for relevant combustion conditions and fuels, thereby yielding a better understanding of the impact of wildfire emissions on climate, regional air quality, and visibility. To serve these objectives, a pilot study in 2003 was followed by FLAME 2006, the first of two major campaigns conducted at the Fire Sciences Lab in Missoula, Montana that involved laboratory measurements of smoke emission composition profiles from several important fuel types. Emission rates and optical, physical, and chemical properties of biomass smoke were also measured in the laboratory setting.

The experimental set up for the chamber burns was as follows: For each of the 19 chamber burns 200 grams of fuel were ignited on a flat flame bed. The smoke from these fires was allowed to fill a large chamber (room with approximate volume of 3,300 m^3) from which two main sample lines drew air to instrumentation located in separate rooms. Sample lines to individual instruments branched off from the primary lines. The sample time for each burn was approximately two hours. Smoke from flaming and smoldering combustion conditions combined to fill the chamber.

The majority of fuels that were burned during the chamber burns are native to the United States and are thought to be representative of wildland fire fuels in different parts of the country. The 14 fuel types analyzed are listed in Table 1 and have been characterized based on vegetation type, with the primary divisions being between coniferous and deciduous flowering plants. Other fuel types include the duffs and those that are more difficult to group, including the fern (not a seed plant) and other miscellaneous flowering plants.

Fuels native to the U.S., including pines, brushes, and decomposing matter from the forest floor (duffs), were burned individually. The smoke from these fires was sampled by instruments measuring aerosol absorption and scattering at different wavelengths, including first measurements by a novel laser-based dual-wavelength photoacoustic instrument. These measurements allow for quantification of the wavelength dependence of absorption according to biomass fuel type. The Ångström exponent of absorption is reported as a function of single scattering albedo for 14 fuels that were individually burned.

3. Instrumentation for Measurement of Aerosol Optical Properties

Aerosol light absorption is most commonly measured by removing suspended particles from the air and depositing them at a known flow rate on a filter. Aerosol light absorption is measured using a radiation source to illuminate the loaded filter and an optical detector to quantify incremental changes in transmittance or reflectance with time. The Particle Soot Absorption Photometer (PSAP) manufactured by Radiance Research, and the Aethalometer by Magee Scientific [*Hansen, et al.*, 1984] are widely used filter-based instruments which produce real-time measurements. Both single and multi-wavelength versions of the Aethalometer are commercially available. A modified version of the PSAP, which measures absorption at three wavelengths (467 nm, 530 nm, and 660 nm) has been developed and calibrated but is not commercially available [*Virkkula, et al.*, 2005]. In these instruments the filter substrate causes multiple scattering enhancement of particle light absorption, amplifying the signal, and thus improving the sensitivity of such measurements. However, multiple scattering in the filter substrate also complicates instrument calibration.

A common instrument for measuring light scattering by aerosols is the integrating nephelometer by TSI Incorporated. The TSI Model 3563 measures total scattering coefficient and backscattering coefficient at three wavelengths: 450, 550, and 700 nm. Operation of the integrating nephelometer is as follows. An air sample is continually drawn through the sample volume and is illuminated over an angle of 7 to 170 degrees by a cosine-weighted diffuse light source. Photomultiplier tubes serve as radiation detectors and view the scattering volume. Light scattered by either a gas or aerosol sample is geometrically integrated over the illumination angle yielding the sample's scattering coefficient [*Anderson, et al.*, 1996]. By comparison, and as discussed in more detail below, light scattering is measured with the photoacoustic instrument in a similar manner using reciprocal nephelometry. In the reciprocal nephelometer design the light source and light detector are exchanged relative to the "normal" design such that a parallel beam (e.g., laser beam) illuminates the sample and a cosine-weighted detector measures scattered optical power.

The photoacoustic instrument measures aerosol light absorption and scattering coefficients directly for airborne particulate matter. It provides an absorption measurement that can be compared to the more commonly used PSAP and Aethalometer, but it is without the filter-based artifacts and resulting correction factors. An evaluation mechanism for calibration of light absorption by the photoacoustic instrument exists in employing light absorbing gases such as nitrogen dioxide [*Arnott, et al.*, 2000]. The large dynamic range of measurement provides another advantage for photoacoustic measurements. Finally, inclusion of scattering measurement along with light absorption within a single instrument allows for calculation of extinction and single scattering

albedo, the most important parameters in aerosol radiative forcing and atmospheric visibility.

4. Dual Wavelength Photoacoustic Instrument

Single wavelength photoacoustic instruments have been used extensively for aerosol light absorption measurements [*Arnott, et al.*, 1999; 2003a; 2003b; 2005; *Arnott and Moosmüller*, 2005; *Lack, et al.*, 2006; *Moosmüller, et al.*, 1998; *Schmid, et al.*, 2006; *Schnaiter, et al.*, 2005; *Sheridan, et al.*, 2005]. This section describes a novel dual wavelength instrument for simultaneous measurement of aerosol scattering and absorption at two wavelengths.

4a. Absorption Measurement

The dual-wavelength photoacoustic instrument employs two power-modulated lasers and allows for simultaneous, in situ measurement of light absorption and scattering by aerosol and gas at the violet wavelength of 405 nm and at the near-infrared (IR) wavelength of 870 nm. Measurements in a single instrument of light absorption and scattering at more than one wavelength are especially useful in determining aerosol properties for rapidly changing plumes. An indication of particle size is provided by dual-wavelength scattering measurements due to the wavelength dependence of scattering by fine particles. In addition, measurement of light absorption at two wavelengths provides insight into the composition of the aerosol sample. BC is expected to strongly absorb across a broad spectral range such that light absorption is inversely proportional to wavelength, while organic carbon aerosol exhibits much stronger light absorption towards the ultraviolet [*Kirchstetter, et al.*, 2004]. Therefore, measurements at violet wavelengths respond not only to the elemental carbon nature of the sample but

also to the presence of organic carbon species, both from primary and secondary sources. Light absorption by rock and mineral dust also has wavelength selective absorption [*Bergstrom, et al.*, 2002].

Dual measurement capabilities of the instrument are also beneficial in instrument operation and applications. The ability for simultaneous measurements makes the dual-wavelength photoacoustic instrument very valuable in applications with relatively short sampling times, and aides in instrument calibration. Because all scattering and absorption measurements are made in a single instrument there is no need to divert sample flow between two instruments operating at different wavelengths, or align two instruments serially and contend with particle loss. Calibration of the absorption measurement on the dual-wavelength photoacoustic instrument is limited to a single microphone calibration and, therefore, is simpler and less error-inducing than additional component calibrations at additional wavelengths.

Additionally, operation at the violet wavelength of 405 nm provides the option of measurement of absorption by nitrogen dioxide gas (NO_2). Measurement of absorption by NO_2 can be used as a calibration method for the photoacoustic signal [*Arnott, et al.*, 2000]. For sufficiently high concentrations of NO_2, extinction, measured from reduced gas transmissivity, is large enough that Rayleigh scattering by the gas molecules can be ignored. Assessment of instrument calibration is then determined by comparison of extinction with measured photoacoustic absorption by the NO_2 sample, without requiring precise knowledge of gas concentration or spectrum.

The laser alignment scheme is shown in the dual-wavelength photoacoustic instrument schematic in Figure 1. The two laser beams are combined outside of the

resonator so that the beams overlap and enter the resonator cavity coincidently. A long wave pass dichroic beamsplitter specified to transmit 850 nm radiation and reflect 400 nm radiation (CVI Laser, LLC product number LWP-45-RS400-TP850-PW-1025-UV) is used for combining the beams. Product specifications for the beamsplitter provide that reflectance is greater than 99.5% at 400 nm, and average transmission is greater than 85%.

The beams of the two lasers employed for the dual-wavelength photoacoustic instrument must both be directed cleanly through the resonator. Unwanted interaction of the laser beams with the resonator walls introduces additional background light scattering and lowers the available laser power for absorption measurement. The lasers are bolted to an aluminum laser alignment plate, and this plate rests on an adjustable platform. Precise knowledge of laser propagation path through the beamsplitter allows for simple beam combination and laser alignment without additional optical elements. Slight manipulation of both the laser/beamsplitter platform as well as minor rotational adjustment of the beamsplitter provide additional control of laser alignment. The windows employed to allow the laser beam to enter and exit the acoustic resonator have a broadband anti-reflective coating that allows strong transmittance of both 405 nm and 870 nm radiation (CVI Laser, LLC product number W2-PW1-1025-UV-670-1064-0).

The primary limiting factor on the sensitivity of photoacoustic measurement is the laser power. More laser power produces more energy absorbed and, therefore, larger acoustic pressure values. The modulated laser power is 93 mW at 405 nm, and is 900 mW at 870 nm. Assuming an inverse wavelength dependence of aerosol light absorption, the 870 nm measurement signal to noise ratio (sensitivity) is 5 times that of the 405 nm

measurement. The 405 nm laser, because it has lower optical power output so that greater absolute efficiency is needed at that wavelength, is reflected by the beamsplitter while the 870 nm beam is transmitted. For maximum efficiency the reflected laser beam is S-polarized (polarized perpendicular to the plane created by normal to beamsplitter surface and laser propagation direction), and the transmitted beam is P-polarized (parallel polarization). The laser beams are aligned perpendicular to each other, and the normal of the beamsplitter surface is aligned at an angle of 45 degrees to the propagation direction of both beams.

On the dual-wavelength photoacoustic instrument, the integrating sphere containing the photodetectors for laser power measurement is positioned so that a mirror is needed to direct into it the laser beams exiting the resonator cavity. This arrangement, in contrast to that of the integrating sphere placed directly in line with the exiting beams, reduces radiation scattered back out of the sphere into the resonator.

Two photodiodes are used within the integrating sphere to measure laser power at each wavelength after the beams exit the resonator. The optical power of the 870 nm laser is such that it would saturate both photodiodes if filters were not used in front of the detectors. A short pass filter with 750 nm cut-off wavelength (Edmund Optics product number NT47-585) reduces the 870 nm radiation reaching the photodiode that measures 405 nm laser power. The optimal set-up would employ a second short pass filter in this position, but the current arrangement uses two absorptive neutral density filters of optical density 0.2 and 0.3 in front of the short pass filter. Another neutral density filter of optical density 1.0 is used in front of the photodiode, which measures 870 nm laser power.

During operation of the photoacoustic instrument, sample air is continuously drawn through an acoustic resonator. The sample air is illuminated by laser radiation that is power modulated at the resonance frequency of the resonator. Radiation is absorbed by aerosol particles within the sample, resulting in particle heating, and due to the very small size and high thermal conductivity of the particles, this heat is rapidly transferred to the surrounding air. A change in pressure is induced by the temperature change of the air. The varying pressure disturbance caused by particle heat transfer is amplified by constructive interference associated with the standing wave in the resonator because the laser is modulated at the acoustic resonance frequency. The pressure fluctuations are measured using a microphone located at an antinode of the resonator. Therefore, aerosol light absorption, manifested by particle heat transfer, is measured by the microphone as an acoustic signal [*Arnott, et al.*, 1999]. Appendix A discusses details of the signal processing used in the dual-wavelength instrument to achieve simultaneous scattering and absorption measurements at two wavelengths.

4b. Scattering Measurement

Light scattering by aerosols is measured in the photoacoustic instrument by the method of reciprocal nephelometry [*Mulholland and Bryner*, 1994]. In a reciprocal integrating nephelometer arrangement a parallel beam of light is used to illuminate a scattering volume, and scattered light is detected by a cosine-weighted detector so that the measured optical power is proportional to the total scattering cross section [*Abu-Rahmah, et al.*, 2006]. Within the instrument the laser beam provides the parallel light source and the cosine-weighted detector is positioned on the resonator to view the center

of the sample cavity. The cosine-weighted sensor is fiber coupled to a photomultiplier tube (PMT).

The coefficient of scattering β_{sca} is calculated using the magnitude of the Fourier transformed functions of PMT signal and laser power at resonance frequency. The expression for determining β_{sca} is given by

$$\beta_{sca} = \alpha \frac{\left| \tilde{P}_{PMT} \right|}{\left| \tilde{P}_{L} \right|}, \qquad \text{(Eq. 3)}$$

where α is a calibration factor determined during instrument calibration. The photomultiplier tube signal is given by $P_{PMT,}$ and P_L is the measured laser power. The magnitudes of these two complex functions of frequency are used in Equation 3. Background measurements of scattering are also made periodically during instrument operation of light scattering by filtered (i.e., particle-free) air within the resonator. The scattering background is subtracted from the PMT signal to produce the reported coefficient of scattering.

5. Results

5a. Aethalometer Analysis

Photoacoustic absorption measurements can be compared to measurements made by the more ubiquitous Aethalometer (Magee Scientific, Berkeley, CA). Light absorption measurements by the dual-wavelength photoacoustic instrument correspond to and supplement the more common instrumentation. Measurements of light absorption, calculated from the change in attenuation of light transmission through a loading filter,

[ΔATN], are converted by the Aethalometer into quantities of black carbon mass concentration. Black carbon mass concentration, *[BC]*, in units of mass per volume is determined using the formula

$$[BC] = \frac{[\Delta ATN]}{\sigma}\frac{A}{F\Delta t}. \qquad \text{(Eq. 4)}$$

The absorption efficiency in units of area per mass is given by σ. F is the volumetric flow rate, A is the sample area over which particulate matter is deposited on the filter, and Δt is the measurement interval (typically two minutes). The manufacturer's calibration assumes that all absorption of light is due to BC. A more descriptive term for the reported Aethalometer measurement, as proposed by *Andreae and Gelencser* [2006], is "equivalent black carbon" concentration, or the amount of BC that would produce the same signal. Absorption efficiency is taken to be a function of inverse wavelength: $\sigma(1/\lambda)$. A model AE-31 "Spectrum" Aethalometer was used during FLAME 2006, which reports BC mass concentration at seven wavelengths: 370, 450, 570, 615, 660, 880, and 950 nm. Determination of *[BC]* at each wavelength is achieved by using an absorption efficiency for BC at a visible wavelength, and extrapolating this value to other wavelengths assuming inverse wavelength dependence.

The variation with time of equivalent BC mass concentration with time measured by three channels of the Aethalometer during FLAME is presented along with light absorption measurements by the dual-wavelength photoacoustic instrument in Figures 2 and 3. Figure 2 exhibits results from a burn of Southern California chamise fuel, and Figure 3 from a burn of Asian rice straw. Chamise and rice straw fuels are presented as

examples because they are representative of diverse aerosols with very different optical properties. The left axis of the figures reports the level of equivalent BC mass concentration, and the right axis refers to the photoacoustic light absorption. Aethalometer wavelengths of 370, 470, and 880 nm are chosen here because they are most representative of the operational wavelengths of the photoacoustic instrument. Figures 2 and 3 are not meant to provide information on the mass-weighted aerosol light absorption efficiency. The gaps in the Aethalometer data are associated with filter changes. The sharply declining "ski slope" behavior comes about because Aethalometer calibration is not based on filter loading. Aethalometers have been found to over predict BC concentration on a fresh filter and under predict it on a loaded filter [*Arnott, et al.*, 2005]. The light absorption signal from the dual-wavelength photoacoustic instrument is without the gaps and sloping behavior of BC mass concentration data, and no assumptions are made regarding absorption efficiency or spectral response of the sample in instrument calibration. Notice that the slight declining trend of the central Aethalometer signal is present in the photoacoustic data as well.

Spectral properties of absorption by chamise smoke are indicated by aerosol measurements in Figure 2. Chamise is a U.S. native flowering shrub that grows in California and Southern Nevada. Chamise smoke is very dark with a single scattering albedo at 405 nm of 0.40 as determined by photoacoustic data. The BC mass concentration reported by the Aethalometer is nearly independent of wavelength, indicating very little spectral variability in absorption properties for this fuel. The Aethalometer calibration assumption of light absorption strictly by BC results in an inverse wavelength dependence of absorption efficiency, which is well represented by

chamise smoke. The Ångström exponent of absorption calculated from Aethalometer measurements between 470 nm and 880 nm is near unity: $b = 1.07$.

Figure 3 depicts BC mass concentration and the photoacoustic absorption signal from burn E of Asian rice straw. Rice straw combustion produces a highly scattering smoke, with a single scattering albedo of $\omega = 0.88$ at 405 nm. In contrast to the chamise smoke, the mass concentration of equivalent BC as reported by the seven-wavelength Aethalometer is significantly different at the three depicted wavelength channels with considerably more BC measured at shorter wavelengths indicating increased light absorption for shorter wavelength radiation. Greater absorption at shorter-wavelength visible and ultraviolet radiation suggests the substantial presence of non-BC aerosol components, which preferentially absorb light at shorter wavelengths, such as organic materials. The Ångström exponent for absorption, as calculated from Aethalometer data at 470 and 880 nm is $b = 2.36$.

5b. Nephelometer and Photoacoustic Analysis

Reciprocal nephelometer (RN) measurements of light scattering in the photoacoustic instrument by biomass smoke can be evaluated along side measurements from the TSI integrating nephelometer (IN). The IN measures light scattering by suspended particles at three visible wavelengths: 450, 550, and 700 nm. Nephelometer data and the RN scattering measurements at 405 nm from the dual-wavelength photoacoustic instrument, along with RN scattering data from a single-wavelength instrument operating at 532 nm, are presented in time series form for the rice straw burn in Figure 4. The IN was corrected for angular nonidealities [*Anderson and Ogren*, 1998] assuming sub-micron particles.

As expected for "small" sub-micron particles, light scattering decreases with increasing incident wavelength. Comparison of RN scattering data with IN measurements in Figure 4 provides verification of photoacoustic instrument calibration and performance. More fluctuation is found in scattering measurements provided by the RNs due to high scattering background for these instruments. RN and photoacoustic measurements of light scattering and absorption are averaged over an entire burn for determination of single scattering albedo and spectral analysis, so effects of measurement uncertainty are minimized.

5c. Spectral Aerosol Absorption by Fuel Type

The dependence of aerosol light absorption on wavelength is parameterized using the Ångström exponent of absorption *b*. This parameter is calculated using β_{abs} measurements at two different wavelengths:

$$b\left(\lambda_1/\lambda_2\right) = -\frac{\ln\left(\beta_{abs}(\lambda_1)/\beta_{abs}(\lambda_2)\right)}{\ln\left(\lambda_1/\lambda_2\right)}, \qquad \text{(Eq. 5)}$$

where λ_1 and λ_2 represent two different radiation wavelengths, and $\beta_{abs}(\lambda_1)$ is the absorption coefficient measured at λ_1. Spectral response is analyzed in light of single scattering albedo, ω. Recall that ω indicates the relative magnitude of scattering versus absorption of an aerosol, and is calculated at λ = 405 nm.

The Ångström exponent *b* and single scattering albedo results, shown in Figures 5 and 6, are derived from photoacoustic measurements of light absorption and scattering from each of the FLAME burns for wavelengths (405 nm and 870 nm) and (532 nm and

870 nm), respectively. The data points represent *b* and ω values calculated from absorption and scattering coefficients averaged over a single two hour chamber burn. The results in Figures 5 and 6 have been grouped and labeled according to fuel characterization. Fuel labels are also provided in the legend. The two figures have matching axes. It is apparent from Figures 5 and 6 that those fuels which produce relatively "dark" aerosol upon combustion with ω values ranging from 0.37 to 0.5 also exhibit *b* values near unity. Aerosols from the combustion of such fuels exhibit optical properties similar to BC or diesel soot. Combustion aerosols with higher single scattering albedos, particularly with values above 0.75 (or corresponding to at least three times as much scattering as absorption by the particles) have Ångström exponents increasingly greater than one. Such fuels show increased absorption at shorter wavelengths. The optical properties of the highly scattering aerosols are not well represented by the BC assumption of absorption efficiency that scales as $1/\lambda$, or *b* equal to one. For example, the Ångström exponent calculated for the rice straw burn is 2.8. This *b* value corresponds to an absorption ratio at wavelengths of 405 and 870 nm, which is nearly four times that expected for inverse-wavelength dependence.

Ångström exponent *b* and ω values presented in Figure 6 were determined using photoacoustic absorption and RN scattering at 532 and 870 nm. The same general trend present in Figure 5 is also apparent in Figure 6. Smoke from fuels producing "dark" combustion aerosols is well represented by an inverse-wavelength absorption dependence model, while this model fails for certain other fuels with increased scattering and Ångström exponents greater than one. Increased *b* values for certain fuels indicate the smoke absorbs short wavelength radiation much more efficiently. The range of

Ångström exponents when determined by signals at 532 and 870 nm is not as great as that by signals at 405 and 870 nm. For example, for rice straw fuel *b(532/870)* = 2.0 and recall *b(405/870)* = 2.8. This indicates much more absorption at the near-UV wavelength of 405 nm than of green radiation at 532 nm.

The results shown in Figures 5 and 6 suggest the presence of non-black carbon components that preferentially absorb light at shorter wavelengths in those fuels with *b* greater than one. Organic materials, which have been shown to strongly absorb radiation at wavelengths shorter than 600 nm [*Kirchstetter, et al.*, 2004], are postulated to be responsible for the increased absorption at shorter wavelengths resulting in increased *b* exponents. Organic species are present in optically relevant quantities in the smoke produced from certain fuels. These smokes generally have much higher albedo than typical BC-dominated light-absorbing aerosols. Assuming optical properties of BC for all light absorbing particulates will introduce large errors for many biomass burning aerosols due to the strong spectral dependence of OC absorption. Casual use of the inverse wavelength dependence, such as in remote sensing data, can result in errors as large as a factor of six in determining UV absorption and a factor of two in the visible when β_{abs} is extrapolated to shorter radiation wavelengths from a single near-IR absorption measurement.

Our division between fuels producing BC-dominated combustion aerosols and those with more complex composition displaying different optical properties is in line with chemical and physical analysis of the smoke aerosol. Using sp^2 hybridization and chemical composition along with optical properties, *Hopkins et al.* [2007] grouped 12 of the biomass fuels into three categories. Representative fuels from these categories

include ponderosa pine from Category 1 which produced combustion aerosol characterized by oily OC with BC inclusions, rice straw from Category 2 producing combustion aerosol containing mixed carbonaceous and inorganic material, and chamise from Category 3 dominated by BC combustion aerosol with some inorganic inclusions [*Hopkins, et al.*, 2007].

6. Conclusion

The spectral response of light absorption for carbonaceous aerosols is quite complex. The simple assumption of inverse wavelength dependence of absorption efficiency generally applied to BC aerosol has been shown to be inaccurate for smoke from the combustion of many biomass fuels. The substantial presence of organic carbon and inorganic components in addition to BC in certain biomass fuel combustion aerosols affects aerosol optical properties. Smoke from these fuels has a higher single scattering albedo than does typical BC aerosol, such as diesel soot. In addition, this smoke exhibits increased absorption at shorter radiation wavelengths due to the presence of light absorbing organic material. In analysis of aerosols from biomass burning in remote sensing and modeling applications, errors will be introduced by the extrapolation of absorption at longer wavelengths to UV or short visible wavelengths under the commonly used assumption that the Ångström exponent of absorption is equal to one.

Biomass fuel classification is suggested by optical properties of the aerosol produced during combustion, based on the spectral response of absorption parameterized by the Ångström exponent b and aerosol single scattering albedo ω. Increased absorption at shorter wavelengths due to organic carbon in the particles and higher ω values separate combustion of many pines, duffs, and rice straw from typical BC-producing fuels used in

mobile or industrial sources, such as diesel fuel. The fraction of organic materials present in smoke from fuels such as the shrubs chamise, manzanita, sage, and rabbitbrush is considerably less than that of elemental carbon. Black carbon optical properties dominate for these dark and sooty fuels.

Appendix A.

The theory of operation of the photoacoustic instrument is described below, including the details of phase-sensitive detection and dual-wavelength operation.

1A. The Photoacoustic Equation and Uncertainties

Light absorption, β_{abs}, measured by the photoacoustic instrument in dimensions of inverse distance, is proportional to the measured microphone power at resonance frequency, $P_m(f=f_o)$, divided by laser power at resonance frequency, $P_L(f=f_o)$. Fourier transforms of both microphone response and laser power measurement transform the time domain signals into complex functions in the frequency domain for determination of microphone and laser power values at the resonance frequency f_o. Fourier analysis of the microphone and laser power signals also allows for phase sensitive detection of the light absorption signal. Light absorption is also a function of resonator cross sectional area, A_{res}, resonator quality factor, Q, and resonance frequency. The full expression for calculating β_{abs} is given by the photoacoustic equation:

$$\beta_{abs} = \frac{P_m}{P_L}\frac{A_{res}}{\gamma - 1}\frac{\pi^2 f_o}{Q}\cos(\phi_M - \phi_L) \qquad \text{(Eq. A1)}$$

where γ is the ratio of isobaric and isochoric specific heats for air. For dry air $\gamma = 1.4$; in general γ is dependent upon relative humidity, but negligibly so in this application. The meaning of the cosine is discussed next.

Fourier transform of the time dependent microphone signal (a measure of absorption-induced pressure fluctuations) and photodiode signal (a measure of laser power) transforms each into a complex function of frequency. The complex values of the

microphone and photodiode signal in the frequency domain are determined at an electronic bandwidth of 1 Hz width centered at the resonance frequency. It is convenient to represent the complex microphone and laser powers at resonance in phasor form, which includes the magnitude (P_m or P_L) and phase (φ_m or φ_L) of the complex value:

$$\text{Complex Microphone Power (at resonance)} \equiv \tilde{P}_m(f_o) = P_m e^{i\phi_m} \qquad \text{(Eq. A2)}$$

$$\text{Complex Laser Power (at resonance)} \equiv \tilde{P}_L(f_o) = P_L e^{i\phi_L} \qquad \text{(Eq. A3)}$$

The measured value of β_{abs} is proportional to the real part of the ratio of complex microphone and photodiode signals,

$$\beta_{abs}(f_o) \sim \mathrm{Re}\left[\frac{\tilde{P}_m(f_o)}{\tilde{P}_L(f_o)}\right] = \mathrm{Re}\left[\frac{P_m e^{i\phi_m}}{P_L e^{i\phi_L}}\right] = \mathrm{Re}\left[\frac{P_m}{P_L} e^{i(\phi_m - \phi_L)}\right] = \frac{P_m}{P_L}\cos(\phi_m - \phi_L) \qquad \text{(Eq. A4)}$$

Therefore, the actual light absorption measurement includes the ratio of microphone and laser power magnitudes at resonance frequency multiplied by the cosine of the difference of microphone and laser signal phases. Any part of the microphone signal that is induced by heat transfer due to light absorption will be in phase with the laser power, its source. Phase sensitive detection is therefore referenced to the frequency of laser power modulation. When the phase difference between the microphone and

photodiode signals is zero the cosine in Equation A4 will be maximized, as will the light absorption signal. Phase sensitive detection of β_{abs} allows the signal due to aerosol light absorption to be separated more effectively from acoustic noise.

Uncertainties in the photoacoustic absorption measurement, not arising from calibration or operator error, result from uncertainties of those parameters that go into determination of β_{abs} (see the photoacoustic equation: Equation A1). Measurement uncertainties of resonance frequency, f_o, resonator quality factor, Q, laser power, P_L, and microphone pressure, P_M, introduce uncertainties in measured absorption. The fractional uncertainty in β_{abs}, or the uncertainty in β_{abs} divided by the absolute value of β_{abs}, is the sum of fractional uncertainties in the measured quantities:

$$\frac{\delta\beta_{abs}}{|\beta_{abs}|} = \frac{\delta P_M}{|P_M|} + \frac{\delta P_L}{|P_L|} + \frac{\delta Q}{|Q|} + \frac{\delta f_o}{|f_o|}. \qquad \text{(Eq. A5)}$$

The fractional uncertainty in microphone pressure is equal to the measured noise of the absorption measurement divided by $|\beta_{abs}|$. When this value is averaged over an entire burn, as it is in the measurements presented in this paper, the error in microphone pressure is very small, so that only the small uncertainties in P_L, f_o, and Q cause error in β_{abs}. A five percent uncertainty exists in the laser power measurement. Resonance frequency can be measured to within 0.2 Hz, and the uncertainty in resonator quality factor measurement is less than one. Assuming typical values of f_o and Q (1500 Hz and 72, respectively) the uncertainty in average absorption values is approximately 0.07 Mm^{-1}.

2A. Dual-Wavelength Photoacoustic Signal Measurement

The operating frequency of the photoacoustic instrument is the temperature and relative humidity-dependent resonance frequency of the resonator cavity. In the single-wavelength instrument, the laser is power modulated at this resonance frequency, and the phase of the Fourier-transformed laser power measurement serves as the reference for phase-sensitive detection. In the dual-wavelength instrument, simultaneous measurement of two light absorption-induced pressure fluctuations is necessary. If both acoustic signals were modulated and analyzed at resonance without phase shift, the resulting microphone pressure would be a combination of the two, and the individual signals could not be separated. Therefore, in the dual-wavelength photoacoustic instrument the 405 nm laser is power modulated at resonance frequency, f_o, and the 870 nm laser is modulated off resonance at f_o+df. The microphone pressure corresponding to one photoacoustic signal is measured at resonance, $P_m(f_o)$, and the other is measured off of resonance, $P_m(f_o+df)$. A typical value for df is five Hz, which is large enough for signal separation but close enough to f_o to still have adequate resonance enhancement of the acoustic pressure fluctuation.

Another important consideration is that calculation of light absorption using the resonance-enhanced microphone pressure in the photoacoustic equation**,** Equation A1**,** assumes that the magnitude of the microphone power is measured at resonance frequency. Consequently, the Fourier-transformed microphone pressure that is measured at f_o+df must be transferred and analyzed as if it occurred at f_o using a transfer function constructed from the theoretical frequency response of acoustic pressure in the resonator. The dependence of resonance-enhanced acoustic pressure on frequency is given by

$$\tilde{P}(f) = \frac{P_o}{\frac{2Q(f - f_o)}{f_o} + i}, \qquad \text{(Eq. A6)}$$

where P_o is the peak acoustic pressure at resonance, and Q is the resonator quality factor. The transfer function is the ratio of Equation A6 evaluated at f_o to the same pressure function measured at a different frequency, for example $f = f_o + df$:

$$\tilde{G}(f - f_o) \equiv \frac{\tilde{P}(f_o)}{\tilde{P}(f)}$$

$$\tilde{G}((f_o + df) - f_o) = \tilde{G}(df) \equiv \frac{P(f_o)}{P(f_o + df)} = 1 - i\frac{2Qdf}{f_o}. \qquad \text{(Eq. A7)}$$

The product of $G(f - f_o)$ and acoustic pressure at some frequency f transfers the acoustic pressure measurement to the value it would have at f_o. The magnitude of the complex transfer function $G(df)$ is

$$G(df) = \sqrt{\left(\frac{2Qdf}{f_o}\right)^2 + 1}, \qquad \text{(Eq. A8)}$$

and the phase of $G(df)$ in radians is

$$\phi_{G(df)} = -\arctan\left[\frac{2Qdf}{f_o}\right]. \qquad \text{(Eq. A9)}$$

Light absorption using a microphone pressure measured off resonance at frequency *f* is proportional to the real part of the ratio of complex microphone power to laser power, both at frequency *f*, multiplied by the transfer function $G(f - f_o)$ as follows:

$$\beta_{abs}(f) \sim \mathrm{Re}\left[\frac{\tilde{P}_m(f)}{\tilde{P}_L(f)}\tilde{G}(f - f_o)\right] = \mathrm{Re}\left[\frac{P_m e^{i\phi_m}}{P_L e^{i\phi_L}} G(f - f_o) e^{i\phi_G}\right]$$

$$= \frac{P_m}{P_L} G(f - f_o)\cos(\phi_m - \phi_L + \phi_G)\,. \qquad \text{(Eq. A10)}$$

Thus, the photoacoustic equation used to measure light absorption at 870 nm in the dual-wavelength photoacoustic instrument is

$$\beta_{abs}(f_o + df) = \frac{P_m(f_o + df)}{P_L(f_o + df)} G(df) \frac{A_{res}}{\gamma - 1} \frac{\pi^2 f_o}{Q} \cos(\phi_m - \phi_L + \phi_G), \qquad \text{(Eq. A11)}$$

and that used to calculate β_{abs} at 405 nm is Equation A11 with *df* equal to zero. In this way independent measurements of light absorption at two different wavelengths are conducted simultaneously within a single photoacoustic resonator. The data acquisition card used for the dual wavelength instrument measures all signals simultaneously.

Acknowledgments

This research was supported in part by grants 0552230 and 0511769 from the National Science Foundation to the Desert Research Institute and the University of Nevada Reno, and in part by the Desert Research Institute through the Applied Research Initiative of the State of Nevada. This work was also supported by the Atmospheric Science Program of the U.S. Department of Energy, Office of Biological and Environmental Research (OBER) and by the Joint Fire Science Program (JFSP) funding FLAME through the US National Park Service (NPS) project #J8R07060005. The authors gratefully acknowledge the staff at the USDA/USFS Fire Sciences Laboratory, along with William C. Malm, Wei-Min Hao, Jeffery L. Collett Jr., and Sonia Kreidenweiss who participated in organizing the FLAME project. Additionally, the authors acknowledge Dr. Grizelle Gonzalez, USDA Forest Service: Sabana Field Research Station, Puerto Rico, Dr. Kevin Robertson, Tall Timbers Research Station, Tallahassee, FL, Joey Chong and Dr. David Weise, USDA Forest Service: Riverside Fire Laboratory and Robert Olson, Utah Air Quality for their contributions of biomass fuels.

1 **References**

2 Abu-Rahmah, A., W. P. Arnott, and H. Moosmüller (2006), Integrating nephelometer
3 with a low truncation angle and an extended calibration scheme, *Meas. Sci. Technol.*, *17*,
4 1723-1732.

5 Anderson, T. L., D. S. Covert, S. F. Marshall, M. L. Laucks, R. J. Charlson, A. P.
6 Waggoner, J. A. Ogren, R. Caldow, R. L. Holm, F. R. Quant, G. J. Sem, A.
7 Wiedensohler, N. A. Ahlquist, and T. S. Bates (1996), Performance characteristics of a
8 high sensitivity, three wavelength, total scatter/backscatter nephelometer, *J. Atmos.*
9 *Oceanic Technol.*, *13*, 967-986.

10 Anderson, T. L., and J. A. Ogren (1998), Determining aerosol radiative properties using
11 the TSI 3563 integrating nephelometer, *Aerosol Sci. Technol.*, *29*, 57-69.

12 Andreae, M. O. (2001), The dark side of aerosols, *Nature*, *409*, 671-672.

13 Andreae, M. O., and A. Gelencser (2006), Black carbon or brown carbon? The nature of
14 light-absorbing carbonaceous aerosols, *Atmos. Chem. Phys. Dis.*, *6*, 3419-3463.

15 Arnott, W. P., K. Hamasha, H. Moosmüller, P. J. Sheridan, and J. A. Ogren (2005),
16 Towards aerosol light absorption measurements with a 7-wavelength Aethalometer:
17 Evaluation with a photoacoustic instrument and a 3 wavelength nephelometer, *Aerosol*
18 *Sci. Technol.*, *39*, 17-29.

19 Arnott, W. P., H. Moosmüller, and J. W. Walker (2003a), Photoacoustic instrument for
20 measuring particles in a gas, Desert Research Institute, Reno NV, USA Patent 6,662,627.

21 Arnott, W. P., and H. Moosmüller (2005), Method and apparatus for photoacoustic
22 measurements, US Patent pending.

23 Arnott, W. P., H. Moosmüller, C. F. Rogers, T. Jin, and R. Bruch (1999), Photoacoustic
24 spectrometer for measuring light absorption by aerosols: Instrument description, *Atmos.*
25 *Environ.*, *33*, 2845-2852.

26 Arnott, W. P., H. Moosmüller, P. J. Sheridan, J. A. Ogren, R. Raspet, W. V. Slaton, J. L.
27 Hand, S. M. Kreidenweis, and J. L. Collett (2003b), Photoacoustic and filter-based
28 ambient aerosol light absorption measurements: Instrument comparisons and the role of
29 relative humidity, *J Geophys. Res.*, *D1*, 4034.

30 Arnott, W. P., H. Moosmüller, and J. W. Walker (2000), Nitrogen dioxide and kerosene-
31 flame soot calibration of photoacoustic instruments for measurement of light absorption
32 by aerosols., *Rev. Sci. Instrum.*, *71*, 4545-4552.

33 Bergstrom, R. W., P. B. Russell, and P. Hignett (2002), Wavelength dependence of the
34 absorption of black carbon particles: Predictions and results from the TARFOX
35 experiment and implications for the aerosol single scattering albedo, *J. Atmos. Sci.*, *59*,
36 567-577.

1 Bond, T. C. (2001), Spectral dependence of visible light absorption by carbonaceous
2 particles emitted from coal combustion, *Geophys. Res. Lett.*, *28*, 4075-4078.

3 Bond, T. C., M. Bussemer, B. Wehner, S. Keller, R. J. Charlson, and J. Heintzenberg
4 (1999b), Light absorption by primary particle emissions from a lignite burning plant,
5 *Environ. Sci. Tech.*, *33*, 3887-3891.

6 Bond, T. C., and H. Sun (2005), Can reducing black carbon emissions counteract global
7 warming? *Environ. Sci. Tech.*, *39*, 5921-5926.

8 Chakrabarty, R. K., H. Moosmüller, W. P. Arnott, M. A. Garro, J. G. Slowik, E. S. Cross,
9 J.-H. Han, P. Davidovits, T. B. Onasch, and D. R. Worsnop (2007), Light scattering and
10 absorption by fractal-like carbonaceous chain aggregates: comparison of theories and
11 experiment, *Appl. Opt.*, *46*, 6990-7006.

12 Chakrabarty, R. K., H. Moosmüller, M. A. Garro, W. P. Arnott, J. Walker, R. A. Susott,
13 R. E. Babbitt, C. E. Wold, E. N. Lincoln, and W. M. Hao (2006), Emissions from the
14 laboratory combustion of wildland fuels: Particle morphology and size, *J Geophys. Res.*,
15 *111*, doi:10.1029/2005JD006659.

16 Charlson, R. J., S. E. Schwartz, J. M. Hales, R. D. Cess, J. A. Coakley, J. E. Hansen, and
17 D. J. Hofmann (1992), Climate forcing by anthropogenic aerosols, *Science*, *255*, 423-429.

18 Crutzen, P. J., and M. O. Andreae (1990), Biomass burning in the tropics: Impact on
19 atmospheric chemistry and biogeochemical cycles, *Science*, *250*, 1669-1678.

20 Hansen, A. D. A., H. Rosen, and T. Novakov (1984), Aethalometer - An instrument for
21 the real-time measurement of optical absorption by aerosol particles, *Sci. Total Environ.*,
22 *36*, 191-196.

23 Hopkins, R. J., K. Lewis, Y. Desyaterik, Z. Wang, A. V. Tivanski, W. P. Arnott, A.
24 Laskin, and M. K. Gilles (2007), Correlations between optical, chemical and physical
25 properties of biomass burn aerosols, *Geophys. Res. Lett.*, *34*,
26 doi:10.1029/2007GL030502.

27 Horvath, H. (1993), Atmospheric Light Absorption - A review, *Atmos. Environ.*, *27A*,
28 293-317.

29 Ito, A., and J. E. Penner (2005), Historical emissions of carbonaceous aerosols from
30 biomass and fossil fuel burning for the period 1870–2000, *Global Biochem. Cyc.*, *19*,
31 doi:10.1029/2004GB002374.

32 Jacobson, M. Z. (2001), Strong radiative heating due to the mixing state of black carbon
33 in atmospheric aerosols, *Nature*, *409*, 695-697.

34 Jones, G. S., A. Jones, D. L. Roberts, P. A. Stott, and K. D. Williams (2005), Sensitivity
35 of global-scale climate change attribution results to inclusion of fossil fuel black carbon
36 aerosol, *Geophys. Res. Lett.*, *32*, doi:10.1029/2005GL023370.

1 Kaufman, Y. J., and R. S. Fraser (1997), The effect of smoke particles on clouds and
2 climate forcing, *Science*, *277*, 1636-1639.

3 Kirchstetter, T. W., T. Novakov, and P. V. Hobbs (2004), Evidence that the spectral
4 dependence of light absorption by aerosols is affected by organic carbon, *J Geophys.*
5 *Res.*, *109*, doi:10.1029/2004JD00499.

6 Lack, D. A., E. R. Lovejoy, T. Baynard, A. Pettersson, and A. R. Ravishankara (2006),
7 Aerosol absorption measurement using photoacoustic spectroscopy: Sensitivity,
8 calibration, and uncertainty developments, *Aerosol Sci. Technol.*, *40*, 697-708.

9 Liu, L., M. I. Mishchenko, and W. P. Arnott (2007), A Study of radiative properties of
10 fractal soot aggregates using the superposition *T*-matrix method, *J. Quant. Spectrosc.*
11 *Radiat. Trans.*, *in press*.

12 Lohmann, U., and J. Feichter (2005), Global indirect aerosol effects: a review, *Atmos.*
13 *Chem. Phys.*, *5*, 715-737.

14 Moosmüller, H., W. P. Arnott, C. F. Rogers, J. C. Chow, C. A. Frazier, L. E. Sherman,
15 and D. L. Dietrich (1998), Photoacoustic and filter measurements related to aerosol light
16 absorption during the Northern Front Range Air Quality Study (Colorado 1996/1997), *J*
17 *Geophys. Res.*, *103, D21*, 28149-28157.

18 Moosmüller, H., S. M. Kreidenweis, J. L. Collett Jr., W. M. Hao, and W. C. Malm
19 (2007), Characterization of Particle Emissions from Laboratory Combustion of Wildland
20 Fuels, *iLEAPS*, *4*, 22-23.

21 Mulholland, G. W., and N. P. Bryner (1994), Radiometric model of the transmission cell-
22 reciprocal nephelometer, *Atmos. Environ.*, *28*, 873-887.

23 Patterson, E. M., and C. K. McMahon (1984), Absorption characteristics of forest fire
24 particulate matter., *Atmos. Environ.*, *18*, 2541-2551.

25 Ramanathan, V., P. J. Crutzen, J. T. Kiehl, and D. Rosenfeld (2001), Aerosols, climate,
26 and the hydrological cycle, *Science*, *294*, 2119-2124.

27 Reid, J. S., R. Koppmann, T. F. Eck, and D. P. Eleuterio (2005), A review of biomass
28 burning emissions part II: intensive physical properties of biomass burning particles,
29 *Atmos. Chem. Phys.*, *5*, 799-825.

30 Schmid, O., P. Artaxo, W. P. Arnott, D. Chand, L. V. Gatti, G. P. Frank, A. Hoffer, M.
31 Schnaiter, and M. O. Andreae (2006), Spectral light absorption by ambient aerosols
32 influenced by biomass burning in the Amazon Basin. I: Comparison and field calibration
33 of absorption measurement techniques, *Atmos. Chem. Phys.*, *6*, 3443-3462.

34 Schnaiter, M., M. Gimmler, I. Llamas, C. Linke, C. Jager, and H. Mutschke (2006),
35 Strong spectral dependence of light absorption by organic particles formed by propane
36 combustion, *Atmos. Chem. Phys. Dis.*, *6*, 1841-1866.

Schnaiter, M., H. Horvath, O. Möhler, K. H. Naumann, H. Saathoff, and W. Schöck (2003), UV-VIS-NIR spectral optical properties of soot and soot-containing aerosols, *J. Aerosol Sci.*, *34*, 1421-1444.

Schnaiter, M., O. Schmid, A. Petzold, L. Fritzsche, K. F. Klein, M. O. Andreae, G. Helas, A. Thielmann, M. Gimmler, O. Mohler, C. Linke, and U. Schurath (2005), Measurement of wavelength-resolved light absorption by aerosols utilizing a UV-VIS extinction cell, *Aerosol Sci. Technol.*, *39*, 249-260.

Sheridan, P. J., W. P. Arnott, J. A. Ogren, B. E. Anderson, D. B. Atkinson, D. S. Covert, H. Moosmüller, A. Petzold, B. Schmid, A. W. Strawa, R. Varma, and A. Virkkula (2005), The Reno aerosol optics study: An evaluation of aerosol absorption measurement methods, *Aerosol Sci. Technol.*, *39*, 1-16.

Sun, H., L. Biedermann, and T. C. Bond (2007), Color of brown carbon: A model for ultraviolet and visible light absorption by organic carbon aerosol, *Geophys. Res. Lett.*, *34*, doi:10.1029/2007GL029797.

Virkkula, A., N. C. Ahlquist, D. S. Covert, W. P. Arnott, P. J. Sheridan, P. K. Quinn, and D. J. Coffman (2005), Modification, calibration and a field test of an instrument for measuring light absorption by particles, *Aerosol Sci. Technol.*, *39*, 68-83.

Figure Captions

Figure 1 Schematic of dual-wavelength photoacoustic resonator and instrument components, including microphone and mounting surrounds, scattering detector, piezoelectric transducer, laser, and photodetector. Two laser beams are combined and directed into the resonator by a long wave pass dichroic beamsplitter.

Figure 2 Aethalometer and dual-wavelength photoacoustic measurements for a burn of chamise fuel. Note the inverse dependence of absorption on wavelength ($\beta_{abs} \sim 1/\lambda$), characteristic of common BC aerosol from diesel engines, for example.

Figure 3 Aethalometer and dual-wavelength photoacoustic measurements for the burn of rice straw fuel. Note the significant spectral variation of light absorption and the Ångström exponent greater than one, indicating light absorbing organic aerosol components in rice straw fuel.

Figure 4 Measurements of aerosol light scattering during FLAME burn of rice straw fuel at five wavelengths by three instruments: two reciprocal nephelometers (RNs) integrated into photoacoustic instruments and a TSI integrating nephelometer (IN). IN measurements were provided by the Missoula Fire Sciences Lab.

Figure 5 Ångström exponent *b(405/870)* versus ω, the ratio of scattering to extinction at 405 nm for individual burns, labeled by fuel type. Fuels with high ω also show increased *b* values and, therefore, a strong spectral dependence of absorption.

Figure 6 Ångström exponent *b(532/870)* versus ratio of scattering to extinction at 532 nm by smoke from each burn, labeled by fuel type. Certain fuels not well-represented by $\beta_{abs} \sim \lambda^{-1}$ assumption typically held for light absorbing BC aerosol.

Table 1. Fuel listing and classification for FLAME 2006 chamber burns

Fuel	**Fuel Characterization**
Ponderosa Pine, dried needles and sticks	conifer (pine)
Lodgepole Pine, needles and twigs	conifer (pine)
Utah Juniper, foliage and sticks	conifer (pine)
Southern Pine, needles	conifer (pine)
Ponderosa Pine duff	duff (pine)
Alaskan Duff (feather moss)	duff
Southern California Manzanita	flowering shrub
Southern California Chamise	flowering shrub
Southeastern Wax Myrtle	flowering shrub
Utah Sage and Rabbitbrush, foliage and sticks	flowering shrub
Southern California Ceanothus	flowering shrub
Southeastern US Palmetto, leaves	miscellaneous flowering plant
Asian Rice Straw (Taiwan)	miscellaneous flowering plant
Puerto Rico Fern	fern

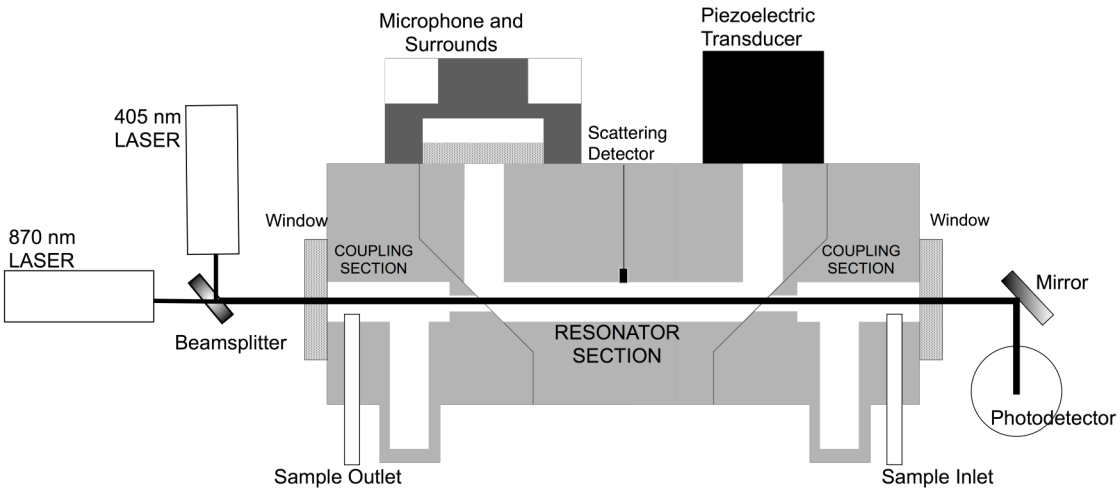

Figure 1 Schematic of dual-wavelength photoacoustic resonator and instrument components, including microphone and mounting surrounds, scattering detector, piezoelectric transducer, laser, and photodetector. Two laser beams are combined and directed into the resonator by a long wave pass dichroic beamsplitter.

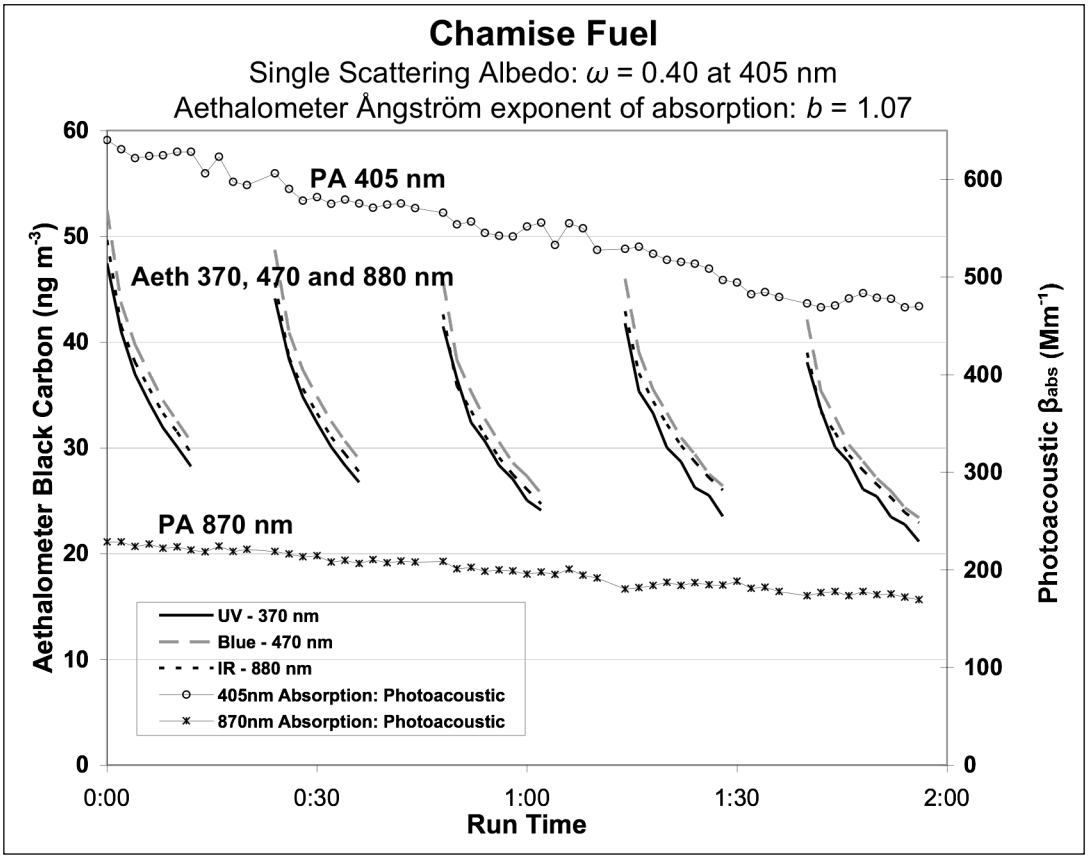

Figure 2 Aethalometer and dual-wavelength photoacoustic measurements for a burn of chamise fuel. Note the inverse dependence of absorption on wavelength ($\beta_{abs} \sim 1/\lambda$), characteristic of common BC aerosol from diesel engines, for example.

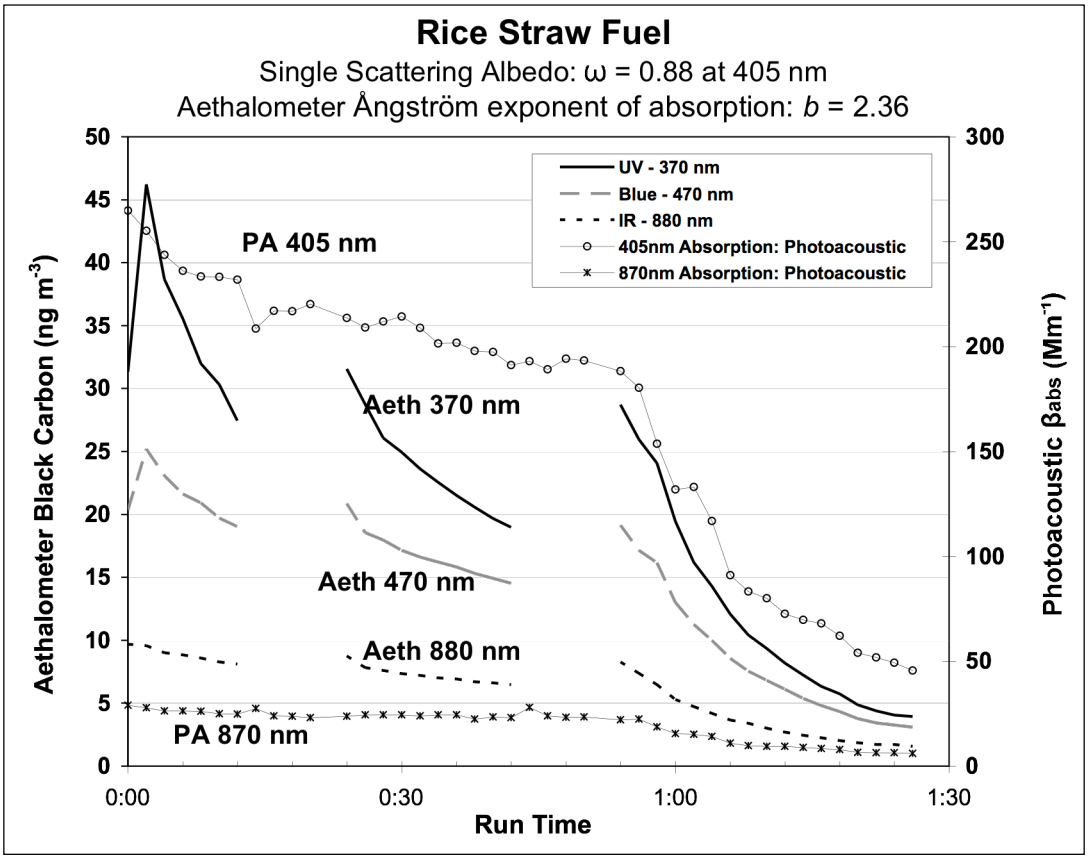

Figure 3 Aethalometer and dual-wavelength photoacoustic measurements for the burn of rice straw fuel. Note the significant spectral variation of light absorption and the Ångström exponent greater than one, indicating light absorbing organic aerosol components in rice straw fuel.

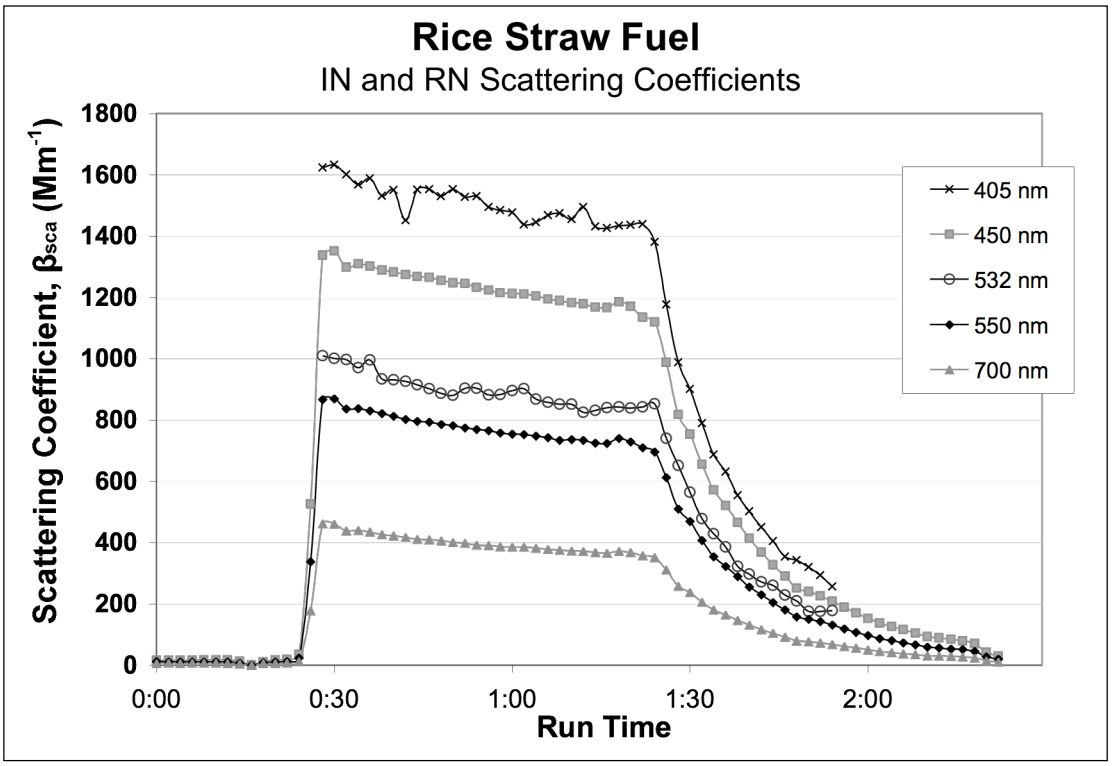

Figure 4 Measurements of aerosol light scattering during FLAME burn of rice straw fuel at five wavelengths by three instruments: two reciprocal nephelometers (RNs) integrated into photoacoustic instruments and a TSI integrating nephelometer (IN). IN measurements were provided by the Missoula Fire Sciences Lab.

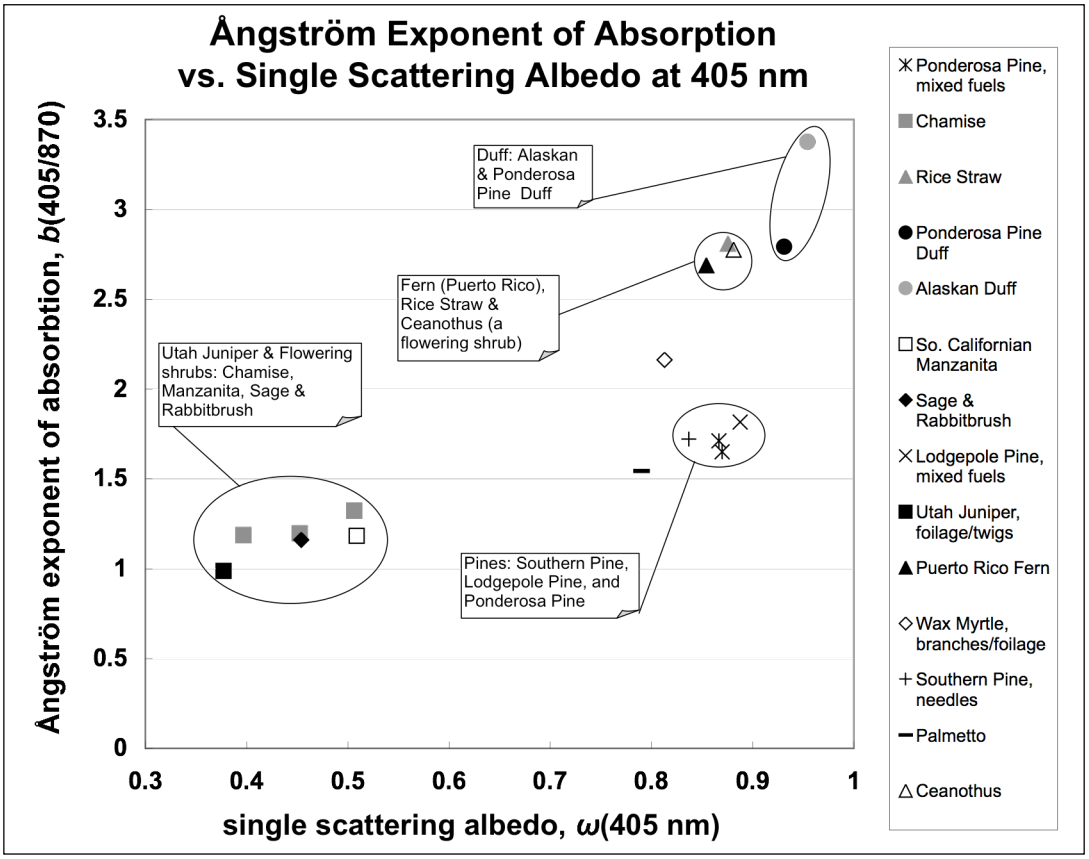

Figure 5 Ångström exponent *b(405/870)* versus ω, the ratio of scattering to extinction at 405 nm for individual burns, labeled by fuel type. Fuels with high ω also show increased *b* values and, therefore, a strong spectral dependence of absorption.

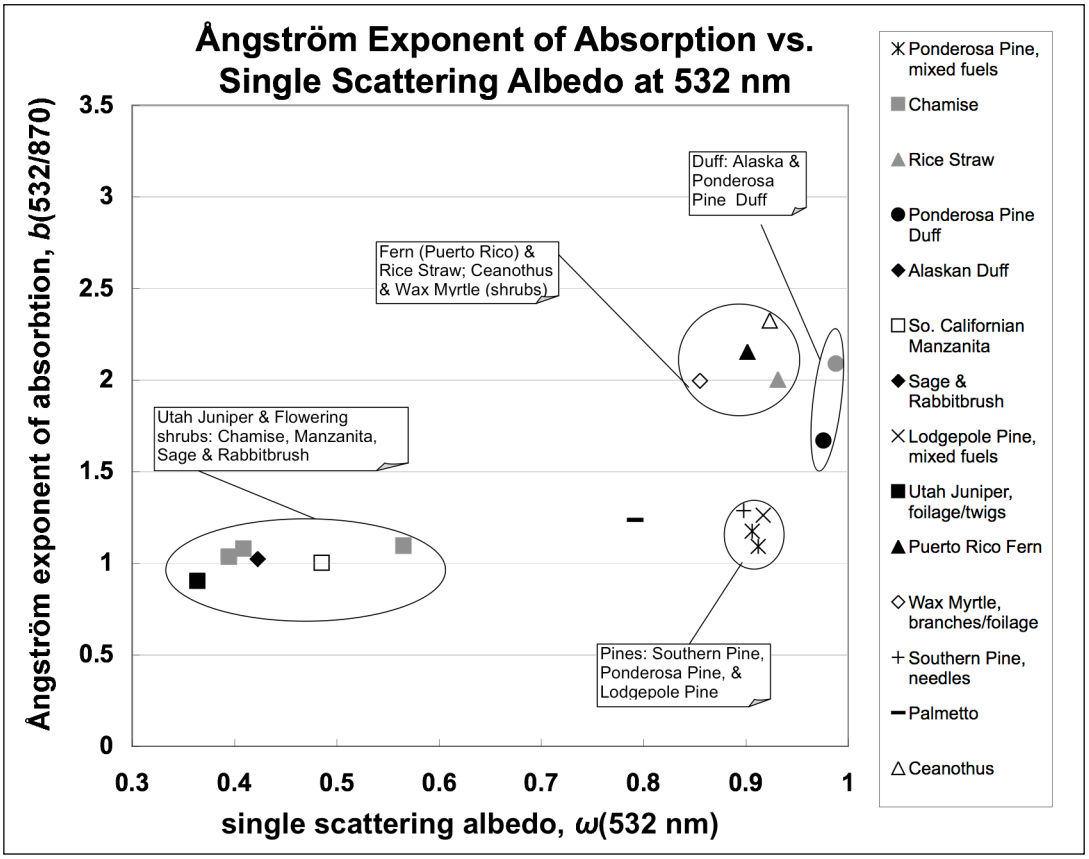

Figure 6 Ångström exponent *b(532/870)* versus ratio of scattering to extinction at 532 nm by smoke from each burn, labeled by fuel type. Certain fuels not well-represented by $\beta_{abs} \sim \lambda^{-1}$ assumption typically held for light absorbing BC aerosol.